Available online at www.sciencedirect.com
SCIENCE DIRECT®
Journal of Power Sources 115 (2003) 161–166
JOURNAL OF POWER SOURCES
www.elsevier.com/locate/jpowsour

Short communication

Mechanically alloyed Mg_2Ni for metal-hydride–air secondary battery

A.A. Mohamad[a], N.S. Mohamed[b], Y. Alias[c], A.K. Arof[a,*]

[a]*Physics Department, University of Malaya, 50603 Kuala Lumpur, Malaysia*
[b]*Center for Foundation Studies in Science, University of Malaya, 50603 Kuala Lumpur, Malaysia*
[c]*Chemistry Department, University of Malaya, 50603 Kuala Lumpur, Malaysia*

Received 28 August 2002; accepted 12 November 2002

Abstract

Mechanically alloyed Mg_2Ni and a single air (oxygen) electrode are used as the anode and cathode, respectively, in a Mg_2Ni|6 M KOH|O_2 rechargeable metal-hydride–air (MH–air) battery. The battery is tested for self-discharge by measuring the open-circuit voltage (OCV) and cycling characteristics. Battery degradation after charge–discharge cycling is characterized by means of X-ray diffraction (XRD) and scanning electron microscopic (SEM) analyses.

Keywords: Metal-hydride–air battery; Mechanical alloying; Mg_2Ni; Air electrode; Self-discharge; Cycling characteristics

1. Introduction

AB_5-type hydrogen-storage alloys, such as $LaNi_5$ [1], $MmNi_{3.6}Co_{0.7}Al_{0.6}Mn_{0.1}$ [2,3], $La_{0.8}Ce_{0.2}Ni_{4.25}Co_{0.5}Sn_{0.25}$ [4] $SrTiO_3$–$LaNi_{3.76}Al_{1.24}H_n$ [5], $MmNi_{3.6}Co_{0.7}Mn_{0.4}Al_{0.3}$ [6] and $MmNi_{3.5}Co_{0.7}Al_{0.7}Mn_{0.1}$ [7], have been reported as negative electrode (anode) for metal-hydride–air (MH–air) systems. AB_5-type anodes have been successfully used for commercial production of nickel–metal-hydride (Ni–MH) batteries, but the capacity of these alloys and product cost are still unsatisfactory. Another family of hydrogen-storage alloys is the A_2B-type, such as Mg_2Ni which has been shown to be a potential candidate for use as an anode material in Ni–MH batteries because of its higher hydrogen-storage capability, lower specific weight and lower cost then commercial $LaNi_5$-based alloys [8–10].

Nickel hydroxide $Ni(OH)_2$ is the positive electrode (cathode) material that is widely used in commercial Ni–MH batteries [11–13]. By replacing the heavy $Ni(OH)_2$ material with a lightweight air electrode, however, it is possible to increase the gravimetric energy density and at the same time reduce cost [14]. In this work, polycrystalline Mg_2Ni alloy prepared by mechanical alloying is used as the anode, a commercial air electrode as the cathode and 6 M KOH as the electrolyte. The open-circuit voltage (OCV) and charge–discharge characteristics of the battery are investigated and failure is investigated by means of X-ray diffraction (XRD) and scanning electron microscopic (SEM) analyses.

1.1. Metal-hydride–air cell chemistry

In general, the charge–discharge reactions for the Ni–MH rechargeable battery using $Ni(OH)_2$ as the cathode, Mg_2Ni as the anode and KOH as the electrolyte solution may be written as [15,16]:

- at the positive electrode:

$$Ni(OH)_2 + OH^- \underset{\text{discharge}}{\overset{\text{charge}}{\rightleftarrows}} NiOOH + H_2O + e^- \quad (1)$$

- at the negative electrode:

$$Mg_2Ni + 4H_2O + 4e^- \underset{\text{discharge}}{\overset{\text{charge}}{\rightleftarrows}} Mg_2NiH_4 + 4OH^- \quad (2)$$

- overall call reaction:

$$4Ni(OH)_2 + Mg_2Ni \underset{\text{discharge}}{\overset{\text{charge}}{\rightleftarrows}} 4NiOOH + Mg_2NiH_4 \quad (3)$$

During the charging process, the $Ni(OH)_2$ at the positive electrode is oxidized to NiOOH, while the alloy M forms MH at the negative electrode. The reactions are reversed during discharging.

The charge–discharge reactions for the MH–air rechargeable battery using an air electrode as the cathode, Mg_2Ni as

* Corresponding author. Tel.: +60-3-79674085; fax: +60-3-79674146.
E-mail addresses: a.azrnin@lycos.com (A.A. Mohamad), akarof@um.edu.my (A.K. Arof).

0378-7753/03/$ – see front matter
PII: S0378-7753(02)00619-5

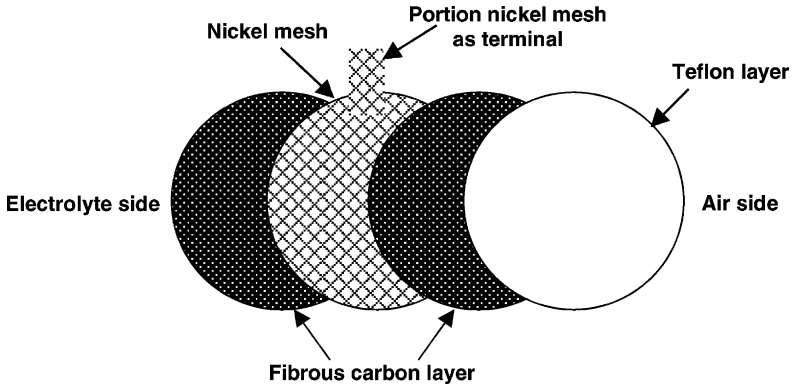

Fig. 1. Laminated air electrode layers.

the anode and KOH as the electrolyte solution proceed as follows:

- at the positive electrode:

$$4OH^- \underset{\text{discharge}}{\overset{\text{charge}}{\rightleftarrows}} O_2 + 2H_2O + 4e^- \quad (4)$$

- at the negative electrode:

$$Mg_2Ni + 4H_2O + 4e^- \underset{\text{discharge}}{\overset{\text{charge}}{\rightleftarrows}} Mg_2NiH_4 + 4OH^- \quad (5)$$

- overall call reaction:

$$Mg_2Ni + 2H_2O \underset{\text{discharge}}{\overset{\text{charge}}{\rightleftarrows}} Mg_2NiH_4 + O_2 \quad (6)$$

During the charge process, oxygen gas is produced by water electrolysis on the air electrode and during the discharge process oxygen gas must be supplied to the air electrode [2,3].

2. Experimental

2.1. Battery components and fabrication

The preparation of Mg_2Ni alloy powder by mechanical alloying takes about 20 days and has been described elsewhere [17]. An amount of 1.5 g of Mg_2Ni alloy and graphite were mixed in a weight ratio of 5:1 and 10 wt.% polyvinyl alcohol (PVA) was added as a binder to form a slurry. The slurry was smeared on to a circular-shaped nickel current-collector to serve as the anode (active area 50.3 cm^2, weight 3.4 g, thickness 0.4 cm). Based on the theoretical specific capacity of Mg_2Ni, viz. 250 mAh g^{-1}, this cell should have a theoretical capacity of about 110 mAh.

The commercial air electrode consists of two active layers bonded to each side of a nickel mesh. The black material, which is a mixture of catalyst (manganese) on carbon fibers and a Teflon binder is also hydrophobic. The white Teflon layer is porous to air but not to water, and is bonded to the air-side of the electrode (see Fig. 1). The air cathode sheet was cut into a circular shape (active area 50.3 cm^2, weight 0.9 g, thickness 0.5 mm).

All battery components were enclosed in a cylindrical plastic casing of dimensions 30 mm (length) and 45 mm (diameter). An electrolyte solution (6 M KOH, volume 35 ml) was poured into the battery casing. The entire battery with electrolyte weighted 66.89 g. A schematic of the design of the $Mg_2Ni|6$ M $KOH|O_2$ battery is shown in Fig. 2.

2.2. Battery characterization

A BAS LG-50 galvanostat system was used to perform constant-current charge–discharge characterization and monitoring of the OCV of the cells. For charge–discharge measurement, the battery was charged at 10.0 mA for 1 h and discharged at 0.1 mA. Self-discharge was investigated by measuring the OCV of the battery after charging and stand at open-circuit for 24 h at 25 °C. Since the battery was charged to 10 mAh, it is not fully charged to its theoretical capacity.

2.3. Electrode characterization

After the battery was cycled, the anode and the cathode were dismantled, cleaned and dried in a desiccator. The

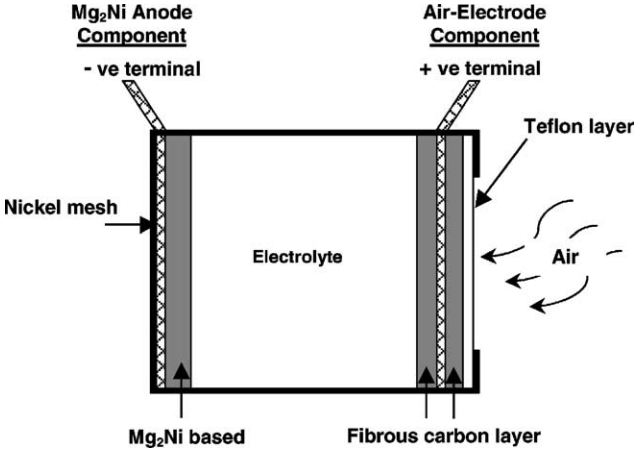

Fig. 2. Cross-sectional view of assembly of MH–air battery from its components.

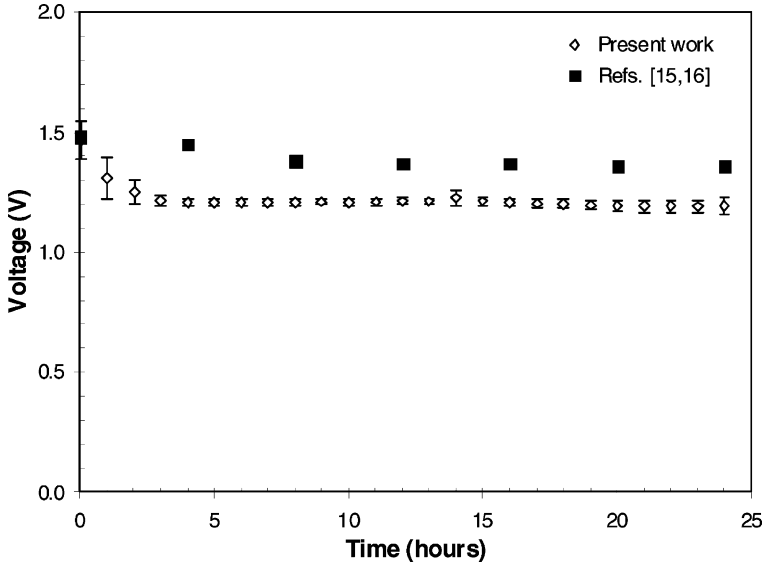

Fig. 3. Open-circuit voltage of Mg_2Ni|6 M KOH|O_2 batteries compared with $Mg_{1.95}Y_{0.05}Ni_{0.92}Al_{0.08}$|6 M KOH–1 M LiOH|Hg/HgO [15,16] during 24 h of storage.

crystallographic features of the electrodes before and after cycling were examined by XRD (Philips X'Pert diffractometer and the surface morphology was observed by SEM (Leica 5440).

3. Result

3.1. Cell characterization

The OCV, shown in Fig. 3, dropped from 1.5 (in the first 2 h) to 1.2 V, and then remained steady at 1.2 V for about 14 h. At the end of 24 h, the OCV is between 1.1 and 1.2 V. Compared with $Mg_{1.95}Y_{0.05}Ni_{0.92}Al_{0.08}$|6 M KOH–1 M LiOH|Hg/HgO [15,16], it can be concluded that additives in Mg_2Ni-based alloys help to improve the OCV by about 0.2 V.

The charge–discharge characteristics are presented in Fig. 4. The longest discharge was observed for cycle 3 and lasted for 8 h. The battery was subjected to 62 cycles. The average charging voltage was about 1.8 V, the average discharge voltages about 0.9 V, and the voltage drop about 0.9 V. Chartouni et al. [7] working with a $MmNi_{3.5-}Co_{0.7}Al_{0.7}Mn_{0.1}$|6 M KOH|$La_{0.6}Ca_{0.4}CoO_3$ battery observed a voltage drop of about 1.1–1.2 V while Gamburzev et al. [4] using a $La_{0.8}Ce_{0.2}Ni_{4.25}Co_{0.5}Sn_{0.25}$|6 M KOH|Hg/HgO cell measured a voltage drop of about 1.0 V.

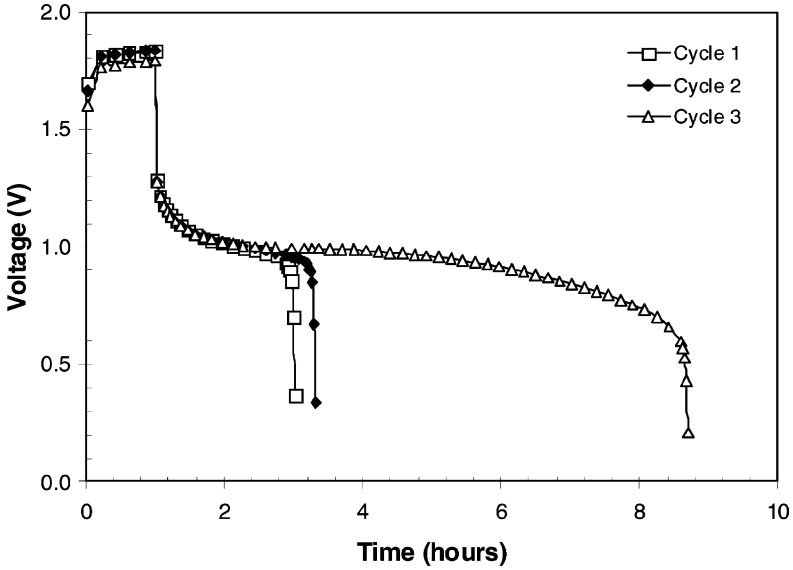

Fig. 4. Charge–discharge curves of Mg_2Ni|6 M KOH|O_2 battery.

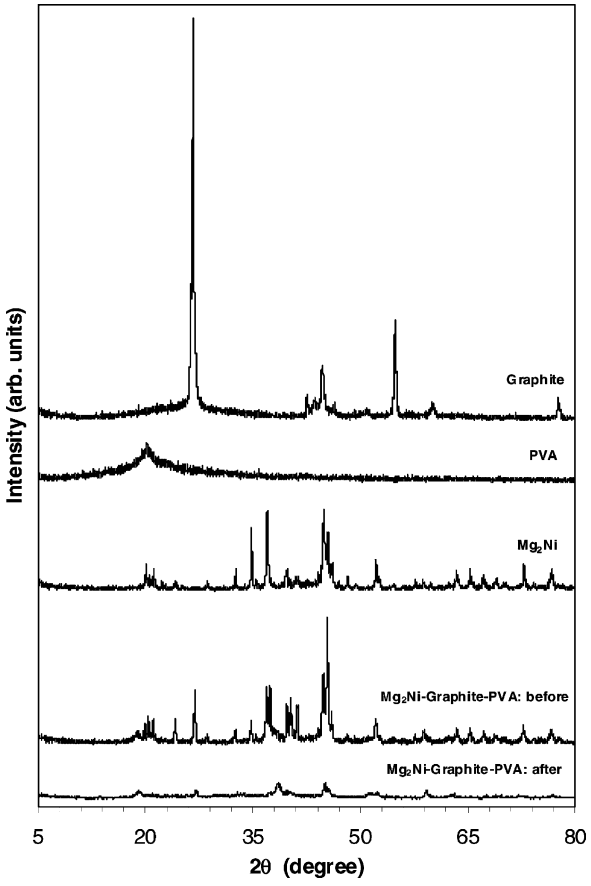

Fig. 5. XRD pattern on anode electrode (graphite additive, PVA binder, Mg_2Ni active material, Mg_2Ni–graphite–PVA) before and after cycling.

Table 1
XRD pattern for cycled Mg_2Ni–graphite–PVA compared with $Mg(OH)_2$ from JCPDS (7-239) data

	2θ (°)								
JCPDS (7-239) data	18.6	32.8	38.0	50.9	58.6	62.1	68.3	68.8	72.0
Present work	19.3	–	38.7	51.5	59.3	62.9	69.2	68.9	72.2

3.2. Electrode characterization

The XRD patterns of materials used in the anode before and after 62 cycles are illustrated in Fig. 5. The Mg_2Ni peaks decrease with cycling and $Mg(OH)_2$ peaks are formed at positions which agree quite well with the values given in JCPDS (7-239) data and [15,16,18,19] (see Table 1), except for the peak at 32.8°.

The thickness of the anode was observed to expand from 0.4 to about 1.0 cm after cycling. This is probably due to the PVA binder in the anode material which had absorbed water from the electrolyte. Electron micrographs of Mg_2Ni–graphite–PVA anode before and after cycling at different magnifications are presented in the Fig. 6a and b, and c and d, respectively. The anode is quite smooth and flat before cycling, but after cycling some portions of the surface become thicker (see Fig. 6d). The thickening of the anode material justifies the above observation of anode expansion.

In order to study the effect of cycling on the air electrode, the fibrous carbon was separated from the nickel mesh. XRD patterns of the Ni mesh, fibrous carbon and air electrode were obtained before cycling. After cycling, the air electrode was again subjected to XRD. The XRD patterns are shown in Fig. 7. The peaks detected at 44.6, 52 and 77° are assigned to

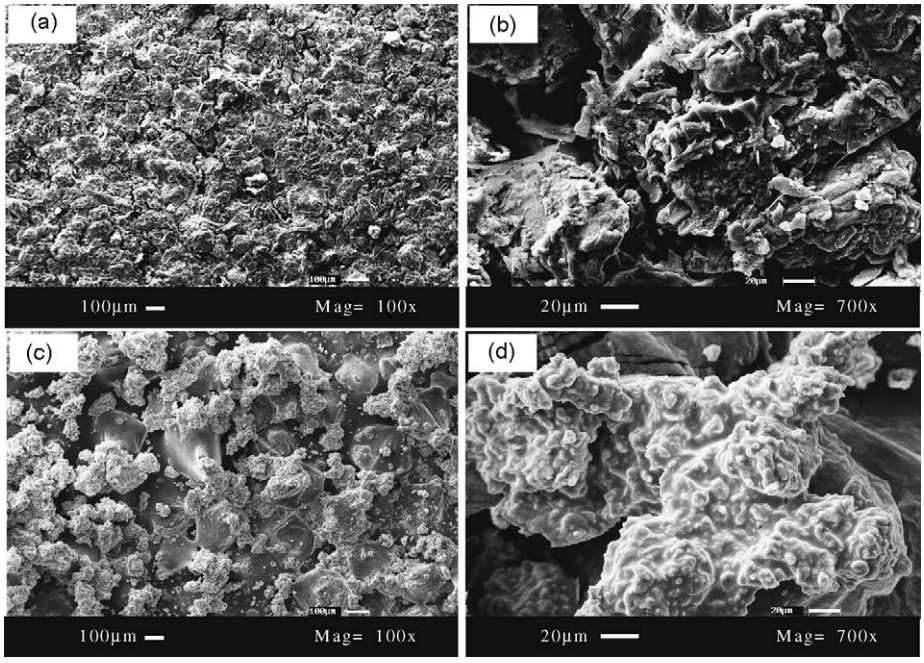

Fig. 6. Scanning electron micrographs of Mg_2Ni–graphite–PVA anode: (a and b) before, and (c and d) after cycling at different magnifications.

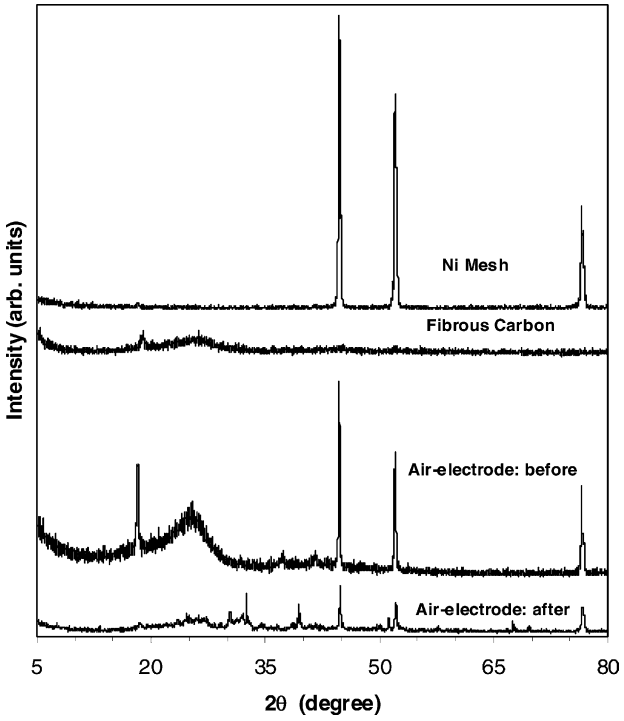

Fig. 7. XRD pattern of air electrode components: Ni mesh, fibrous carbon and air electrode before and after cycling.

nickel mesh, whereas the 18.5° peak is attributed to the fibrous carbon material. The intensities of these peaks reduce significantly after cycling. The XRD pattern of the air cathode after 62 cycles also shows the presence of phases at 30.5, 32.6, 38.9, 39.4, 52.0 and 67.7°. Electron micrographs of the air electrode are given in Fig. 8a and b which shows the catalyst covering the surface of the electrolyte side. In Fig. 8c and d it can be seen that the catalyst at the surface has peeled off after cycling.

4. Discussion

The self-dehydriding of the Mg_2Ni anode during storage probably decreases with increasing storage time following the reduction in the OCV, as shown in Fig. 3. The voltage decreases rapidly during the initial stage of storage in the first 2 h, but slowly thereafter. Luo and co-workers [15,16] reported that the self-dehydriding of a Mg_2Ni-based anode is mainly responsible for a high self-discharge rate. The high self-discharge rate from ~1.5 to 1.2 V of a Mg_2Ni|6 M KOH|O_2 cell is almost the same at that for $Mg_{1.95}Y_{0.05}Ni_{0.92}Al_{0.08}$|6 M KOH–1 M LiOH|Hg/HgO [15,16]. Mg_2Ni-based cells exhibit much higher self-discharge rates than other Ni-MH batteries with AB_5-type anodes [20,21]. The plateau time of the charge–discharge characteristics increases during the first three cycles. This suggests that activation of the alloy surface occurs during initial cycling [18].

The XRD data show that failure of the battery is due to oxidation of the active material Mg_2Ni to form $Mg(OH)_2$. The Mg_2Ni alloy is easily oxidized, especially when it comes into contact with the highly corrosive electrolyte. Rapid degradation during the charge–discharge process hampers a continuous reaction with hydrogen and results in a decay in capacity [10,19,22–24]. The formation of $Mg(OH)_2$ may be represented by the following reaction [23]:

$$Mg_2Ni + 4OH^- = 2Mg(OH)_2 + Ni + 4e^- \quad (7)$$

It has been reported [25,26] that the discharge capacity and cycle-life of the Mg_2Ni–graphite anode are much better than

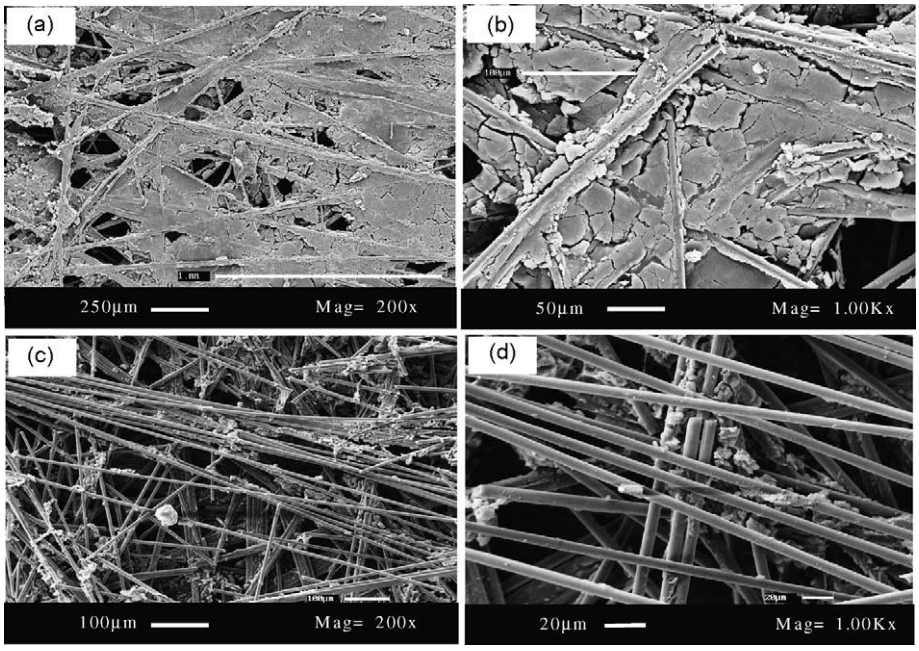

Fig. 8. Scanning electron micrographs of air electrode: (a and b) before, and (c and d) after cycling at different magnifications.

those of a Mg_2Ni anode. Hence, the Mg_2Ni alloy was mixed with graphite in the present study. The XRD intensity of graphite reduces on cycling, however, due to the dissolution of graphite powder into the electrolyte. This causes the electrolyte to turn black and affects the cycle-life of the battery.

The morphology of the Mg_2Ni anode before and after cycling indicates some change in electrode thickness. This may be attributed to the formation of $Mg(OH)_2$ during cycling. It is well known [12,27–29] that the hydrogen absorbing and desorbing cycles bring about pulverization of the alloy continuous enlargement of the surface area, production of a fresh surface, and the formation of oxide or hydroxide. Therefore, repeated charging and discharging in KOH solution causes continuous degradation of the alloy. The thickness of the anode may be attributed to water absorption by PVA, which is known to be water soluble [30,31]. PVA utilized as a binder probably absorbs water after contact with aqueous KOH electrolyte. PVA may be re-dissolved to form a smooth surface film.

The XRD and SEM results also indicate that the failure of the battery is due to changes in the air electrode upon cycling. It has been reported [3,4,6] that the main problem of the single air electrode is its unsuitability for use as a charging electrode. Degradation of the air electrode affects its performance in rechargeable metal–air batteries [32–34].

5. Conclusions

The failure of a battery using mechanically alloyed Mg_2Ni can be attributed to anode degradation to $Mg(OH)_2$ and air electrode damage upon cycling. Battery failure can also be due to thickening of the anode which might exert excess stress on the anode|current-collector interface. The voltage drop on discharge is rapid compare with other systems using air electrodes and mixed rare-earth metal anodes. The capacity is low because the battery is not fully charged.

Acknowledgements

One author (AAM) is grateful to the IRPA University of Malaya for a Pascasiswazah scholarship and vote FO144/2002C to perform this study.

References

[1] J. Sarradin, G. Bronoel, A.P. Guegan, J.C. Achard, in: J. Thompson (Ed.), Power Sources, vol. 7, Academic Press, New York, 1979, pp. 345–351.
[2] T. Sakai, T. Iwaki, Z. Ye, D. Noreus, O. Lindstrom, in: P.D. Bennett, T. Sakai (Eds.), Proceedings of the Electrochemical Society on Hydrogen and Metal Hydride Batteries, vol. 94-27, Pennington, NJ, 1994, pp. 393–402.
[3] T. Sakai, T. Iwaki, Z. Ye, D. Noreus, O. Lindstrom, J. Electrochem. Soc. 142 (1995) 4040.
[4] S. Gamburzev, W. Zhang, O.A. Velev, S. Srinivasan, A.J. Appleby, A. Visintin, J. Appl. Electrochem. 28 (1998) 545.
[5] K. Akuto, Y. Sakurai, J. Electrochem. Soc. 48 (2001) A121.
[6] W.K. Hu, Z. Ye, D. Noreus, J. Power Sources 102 (2001) 35.
[7] D. Chartouni, K. Kuriyama, T. Kiyobayashi, J. Chen, J. Alloys Compd. 330–332 (2002) 766.
[8] C. Iwakura, S. Hazui, H. Inoue, Electrochim. Acta 41 (1996) 471.
[9] J.L. Luo, N. Cui, J. Alloys Compd. 264 (1998) 299.
[10] X. Jianshe, L. Guoxun, H. Yaoqin, D. Jun, W. Chaoqun, H. Guangyong, J. Alloys Compd. 307 (2000) 240.
[11] G. Sandrock, in: P.D. Bennett, T. Sakai (Eds.), Proceedings of the Electrochemical Society on Hydrogen and Metal Hydride Batteries, vol. 94-27, Pennington, NJ, 1994, pp. 1–15.
[12] G. Sandrock, J. Alloys Compd. 293–295 (1999) 877.
[13] D. Linden, in: D. Linden (Ed.), Handbook of Batteries, second ed., McGraw-Hill, New York, 1994, pp. 33.1–33.29.
[14] R.P. Hamlen, in: D. Linden (Ed.), Handbook of Batteries, second ed., McGraw-Hill, New York, 1994, pp. 38.1–38.45.
[15] N. Cui, J.L. Luo, Electrochim. Acta 45 (2000) 3973.
[16] N. Cui, J.L. Luo, K.T. Chuang, J. Alloys Compd. 302 (2000) 218.
[17] A.A. Mohamad, N.S. Mohamed, Y. Alias, A.K. Arof, J. Alloys Compd. 337 (2002) 208.
[18] K. Watanabe, W.M. Shu, K. Mizukami, K. Kobayashi, Y. Hatano, S. Morozumi, J. Alloys Compd. 293–295 (1999) 626.
[19] N.H. Goo, J.H. Woo, K.S. Lee, J. Alloys Compd. 288 (1999) 286.
[20] M. Ikoma, Y. Hoshina, I. Matsumoto, C. Iwakura, J. Electrochem. Soc. 143 (1996) 1904.
[21] C. Iwakura, Y. Kajiya, H. Yoneyama, T. Sakai, K. Oguro, H. Ishikawa, J. Electrochem. Soc. 136 (1989) 1351.
[22] N. Cui, J.L. Luo, Int. J. Hydrogen Energy 24 (1999) 37.
[23] W. Liu, Y.Q. Lei, D. Sun, J. Wu, Q.D. Wang, J. Power Sources 58 (1996) 243.
[24] X.L. Wang, N. Haraikawa, S. Suda, J. Alloys Compd. 231 (1995) 397.
[25] C. Iwakura, S. Nohara, H. Inoue, Y. Fukumoto, J. Chem. Soc., Chem. Commun. (1996) 1831–1832.
[26] H. Inoue, T. Ueda, S. Nohara, N. Fujita, C. Iwakura, Electrochim. Acta 43 (1998) 2215.
[27] J.J. Reilly, G.D. Adzic, J.R. Johnson, T. Vogt, S. Mukerjee, J. McBreen, J. Alloys Compd. 293–295 (1999) 569.
[28] N. Cui, P. He, J.L. Luo, Electrochim. Acta 44 (1999) 3549.
[29] N. Cui, B. Luan, H.K. Liu, H.J. Zhao, S.X. Dou, J. Power Sources 55 (1995) 263.
[30] J.G. Pritchard, Polyvinyl Alcohol: Basic Properties and Uses, Macdonald Technical & Scientific, London, 1970.
[31] M.K. Lindemann, in: H.F. Mark, N.G. Gaylord (Eds.), Encyclopedia of Polymer Science and Technology, vol. 14, Wiley, New York, 1971, pp. 149–207.
[32] S. Müller, K. Straiebel, O. Haas, Electrochim. Acta 39 (1994) 1661.
[33] O. Haas, F. Holzer, S. Müller, J.M. McBreen, X.Q. Yang, X. Sun, M. Balasubramanian, Electrochim. Acta 47 (2002) 3211.
[34] M. Bursell, M. Pirjamali, Y. Kiros, Electrochim. Acta 47 (2002) 1651.